Quantifying exchange in MWI

Jeffrey A. Fessler

EECS Department, BME Department, Dept. of Radiology
University of Michigan

http://web.eecs.umich.edu/~fessler

EPFL Seminar
2022-09-16

Joint work with Naveen Murthy,
Jon Nielsen, Nicole Seiberlich, Scott Swanson, Steven Whitaker

Outline

MRI overview

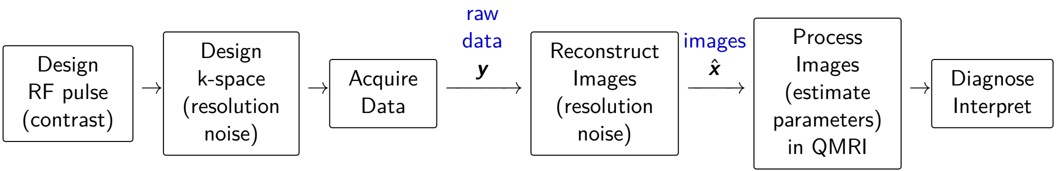

MRI overview

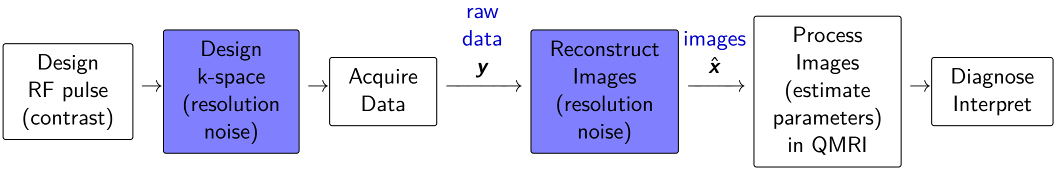

Previous EPFL talk 2022-04-21

`https://www.youtube.com/watch?v=sLFOf5EvVAs`

Guanhua Wang et al., *IEEE TMI*, 2022; arXiv 2101.11369. [1, 2]

MRI overview

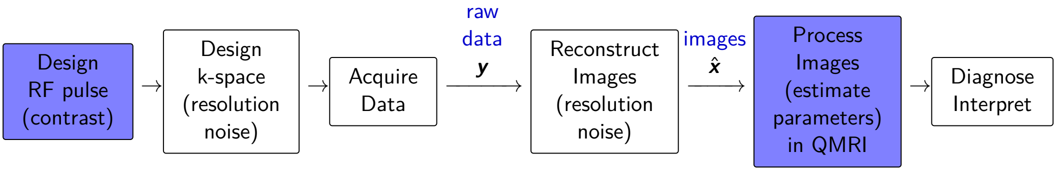

Naveen Murthy et al., ISMRM 2022 #2068 [3]

Qualitative vs. Quantitative MRI

Qualitative or
contrast-weighted images

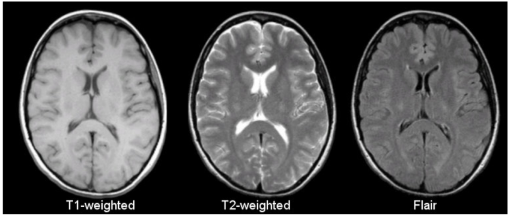

Quantitative parameter
maps

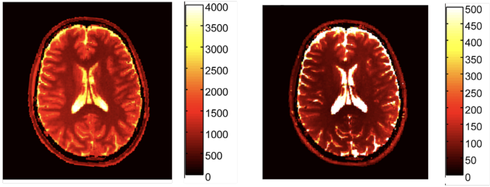

T1 map (in ms) T2 map (in ms)

Image credit: `https://case.edu/med/neurology/NR/MRI%20Basics.htm` and Y. Jiang et al., *MRM*, 2015. [4]

Note: T_1 and T_2 are tissue properties that characterize the nuclear spins' return to equilibrium (after excitation).

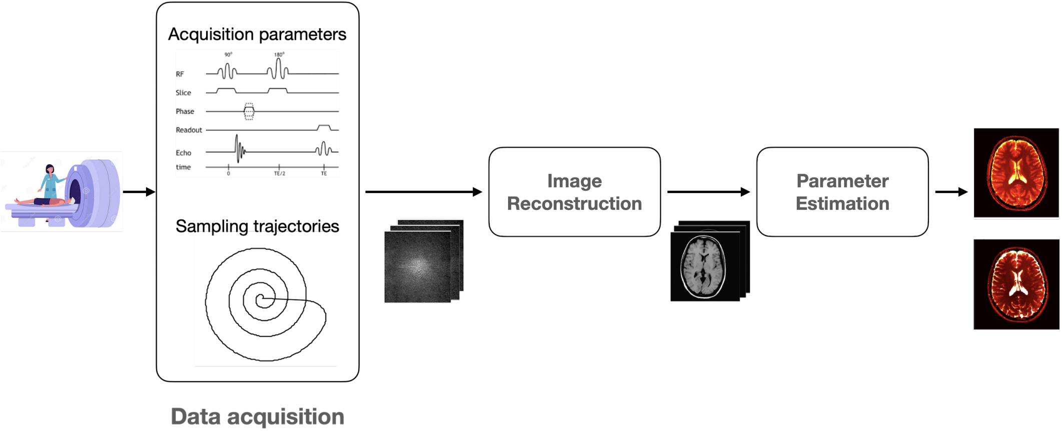
Acquisition parameters
90°
180°
RF
Slice
Phase
Readout
Echo
time
0
TE/2
TE
Sampling trajectories
Image Reconstruction
Parameter Estimation
Data acquisition

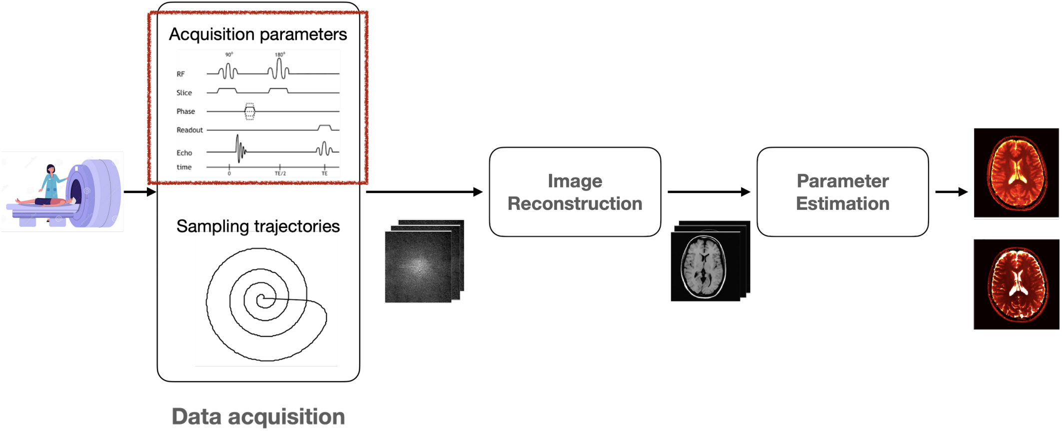
Acquisition parameters
90°
180°
RF
Slice
Phase
Readout
Echo
time
0
TE/2
TE
Sampling trajectories
Image Reconstruction
Parameter Estimation
Data acquisition

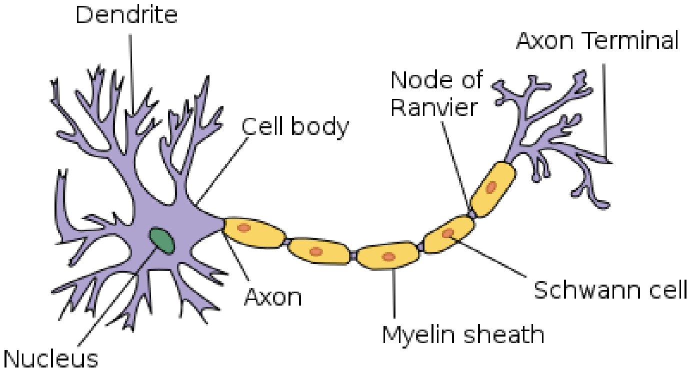

- Insulating sheath surrounding axons in our nervous system
- Enables rapid communication of electric signals along nerves

---

Image credit: User:Dhp1080 CC BY-SA 3.0 via Wikimedia Commons

Demyelination

Loss of myelin (demyelination) is a feature of:

- Multiple sclerosis[1]
- Alzheimer's disease and dementia[2]
- Parkinson's disease[3]
- and more . . .

[1] R. Höftberger and H. Lassmann, *Handbook of Clinical Neurology*, 2018.
[2] M. Bouhrara et al., *Alzheimer's & Dementia*, 2018.
[3] D. C. Dean et al., *PLoS One*, 2016. [5]

Demyelination

Loss of myelin (demyelination) is a feature of:

- Multiple sclerosis[1]
- Alzheimer's disease and dementia[2]
- Parkinson's disease[3]
- and more . . .

How do we track loss of myelin?

[1] R. Höftberger and H. Lassmann, *Handbook of Clinical Neurology*, 2018.
[2] M. Bouhrara et al., *Alzheimer's & Dementia*, 2018.
[3] D. C. Dean et al., *PLoS One*, 2016. [5]

Myelin water imaging (MWI)

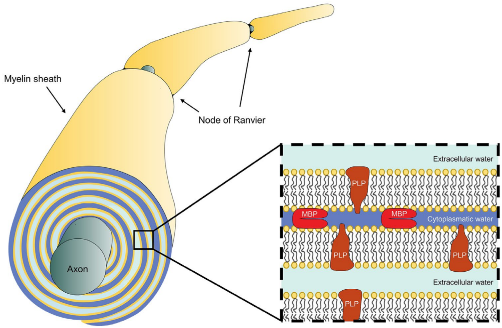

- *Myelin water* : water trapped within myelin sheath;
- *Non-myelin water* : all other water
- Myelin water fraction (MWF) - fraction of total MR signal arising from *myelin water*
- MWF shown to correlate with true myelin content[4]

Image credit: G. F. Piredda et al., *MRM*, 2021. [6]

[4]C. Laule and G. R. W. Moore, *Brain Pathology*, 2018.

Myelin water exchange

- Standard myelin water imaging ignores *exchange* between myelin water and non-myelin water called myelin water exchange.
- Water exchange may be a useful clinical biomarker[5,6].
  Perhaps also in myelin?
- Conventional MWF methods *underestimate* true myelin content in the presence of *exchange*[7,8].

Goal

How do we characterize/measure these exchange dynamics in myelin water imaging?

---

[5] W. Huang et al., *PNAS*, 2008. [7]
[6] S. Kim et al., *JMRI*, 2007. [8]
[7] A. N. Dula et al., *MRM*, 2010. [9]
[8] K. D. Harkins et al., *MRM*, 2012. [10]

Related work: Exchange mapping

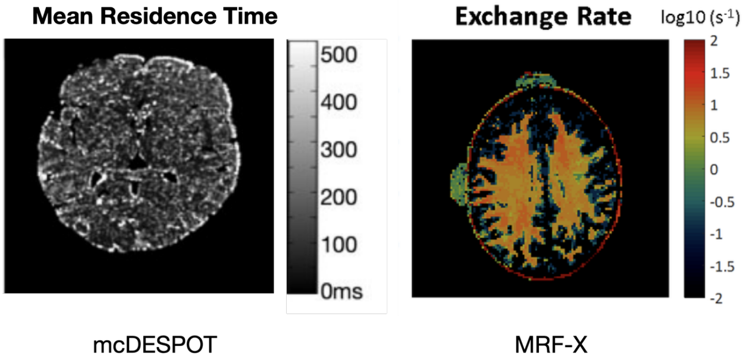

- Previous approaches: mcDESPOT[9], MRF-X[10], REXSY[11]
- No established baseline methods/ground truth
- Challenging to estimate exchange *in vivo*

[9] S. C. L. Deoni et al., *MRM*, 2008. [11]
[10] J. I. Hamilton et al., *Proc. ISMRM*, 2016. [12]
[11] R. D. Dortch et al., *MRM*, 2013. [13]

Single-compartment tissue model:

- Assumes that MR signal in a voxel arises from a *single* type of tissue
- Assumes that all spins in a voxel share MR characteristics (T_1, T_2 etc.)

Multi-compartment tissue model:

- Assumes that MR signal in a voxel arises from various tissue pools/compartments
- Suitable for modeling complex microstructure in living tissues
- We model myelinated tissue using two pools:
  (myelin water and non-myelin water)

Two-pool model for myelinated tissue

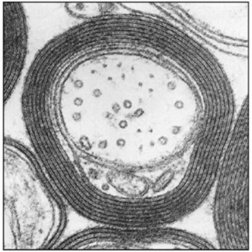

Myelinated tissue

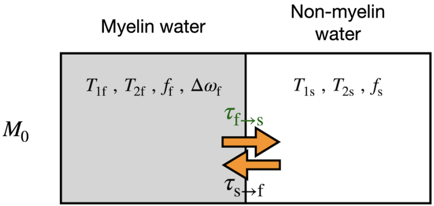

Two pool exchanging model

Assume: $f_f + f_s = 1, \quad \frac{f_f}{f_s} = \frac{\tau_{f\to s}}{\tau_{s\to f}}$ (well mixed).

Image credit: Laule & Moore, *Brain Pathology*, 2018. [14]

Two pool exchanging model

Compartments:

- Fast-relaxing *myelin water* (f)
- Slow-relaxing *non-myelin water* (s); includes intra + extra cellular water

[12] S. Wharton and R. Bowtell, *PNAS*, 2012. [15]

Two pool exchanging model

Compartments:

- Fast-relaxing *myelin water* (f)
- Slow-relaxing *non-myelin water* (s); includes intra + extra cellular water

Parameters:

- Equilibrium magnetization M_0
- Myelin water fraction f_{f}
- Relaxation time constants $T_{1\mathrm{f}}$, $T_{1\mathrm{s}}$, $T_{2\mathrm{f}}$, $T_{2\mathrm{s}}$
- Frequency shift specific to myelin water $\Delta\omega_{\mathrm{f}}$[12]
- Mean residence time of myelin water $\tau_{\mathrm{f}\to\mathrm{s}}$
- Bulk off-resonance $\Delta\omega$
- Flip angle inhomogeneity κ

[12] S. Wharton and R. Bowtell, *PNAS*, 2012. [15]

Mean residence time of myelin water ($\tau_{f \to s}$)

- Mean residence time is the inverse of exchange rate
  (e.g., $\tau_{f \to s} = 150\mathrm{ms}$ corresponds to an exchange rate of $\sim$ 6.7s^{-1}) .
- High value of $\tau_{f \to s} \implies$ *slower* exchange from myelin water to non-myelin water.

Goal:
Design a set of MR acquisitions to estimate exchange ($\tau_{f \to s}$) with good precision.

Outline

Balanced Steady-State Free Precession (bSSFP)

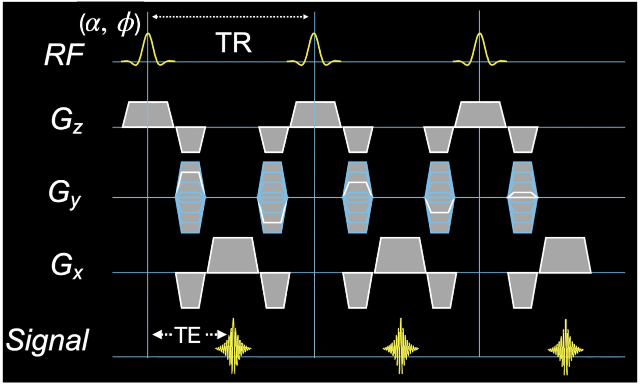

- Rapid train of RF-pulses with *balanced* gradients in each T_{R}
- α - Flip angle, ϕ - RF phase cycling increment factor
- Possibly useful for quantifying exchange? (*cf.* mcDESPOT)

---

bSSFP sequence image from Dr. Brian Hargreaves.

bSSFP signal profiles for two-pool model

Effect of varying flip angle α ($M_0 = 1$, $\Delta\omega_{\mathrm{f}} = 5$ Hz, $T_{\mathrm{R}} = 10$ ms, $\phi = \pi$):

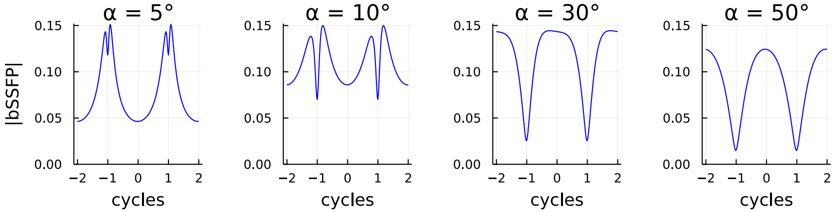

Effect of varying RF phase cycling factor ϕ. ($\alpha = 30°$):

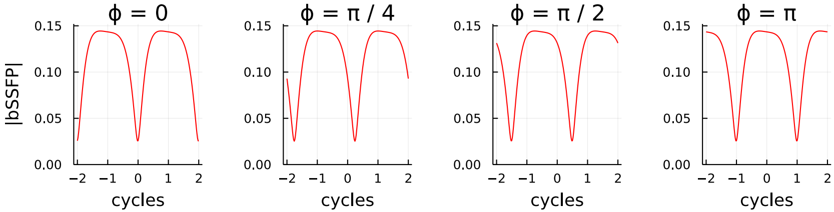

Asymmetry!

Scan design:

- Cramér-Rao bound based optimization for estimating exchange
- Optimize flip angles α and RF phase cycling factors ϕ of a set of bSSFP acquisitions

Estimation:

- Parameter Estimation via Regression with Kernels (PERK)[13]
- Lifts measurements to a higher-dimensional space followed by ridge regression
- Dictionary-free approach suitable for large latent parameter dimensions

[13] Nataraj et al., *IEEE TMI*, 2018. [16]

Goal

Design a set of D fully sampled bSSFP acquisitions to estimate exchange with good precision.

Signal model:

$$\boldsymbol{y}_d = \boldsymbol{s}(\boldsymbol{x}, \boldsymbol{\nu}, \boldsymbol{p}_d) + \boldsymbol{\epsilon}_d, \qquad d = 1, 2, \dots D.$$

- $\boldsymbol{x} \in \mathbb{R}^L$: Unknown tissue parameters $(M_0, f_{\mathrm{f}}, T_{1\mathrm{f}}, T_{1\mathrm{s}}, T_{2\mathrm{f}}, T_{2\mathrm{s}}, \Delta\omega_{\mathrm{f}}, \tau_{\mathrm{f}\to\mathrm{s}})$
- $\boldsymbol{\nu} \in \mathbb{R}^K$: Known parameters $(\Delta\omega, \kappa)$
- $\boldsymbol{p}_d$: Scan parameters $(\alpha, \phi, T_{\mathrm{R}}, T_{\mathrm{E}})_d$
- Example: $L = 8$, $K = 2$, $D = 40$ scans

Cramér-Rao bound

$$\mathrm{Var}\{\hat{\boldsymbol{x}}_i(\boldsymbol{y})\} \geq [\mathbf{F}^{-1}(\boldsymbol{x}, \boldsymbol{\nu}, \boldsymbol{P})]_{(i,i)}$$

- Covariance of any unbiased estimator $\hat{\boldsymbol{x}}(\boldsymbol{y})$ is bounded below by the CRB.
- $\boldsymbol{P} = (\boldsymbol{p}_1, \boldsymbol{p}_2, \ldots, \boldsymbol{p}_D)$ collects all scan parameters.

Fisher information matrix:

$$\mathbf{F}(\boldsymbol{x}, \boldsymbol{\nu}, \boldsymbol{P}) = \frac{1}{\sigma^2} \underbrace{(\nabla_{\boldsymbol{x}}\, \boldsymbol{s}(\boldsymbol{x}, \boldsymbol{\nu}, \boldsymbol{P}))}_{L \times D\ (8 \times 40)} \underbrace{(\nabla_{\boldsymbol{x}}\, \boldsymbol{s}(\boldsymbol{x}, \boldsymbol{\nu}, \boldsymbol{P}))^T}_{D \times L\ (40 \times 8)}$$

Optimization problem:

$$\hat{\boldsymbol{P}} = \operatorname*{arg\,min}_{\boldsymbol{P} \in \mathcal{P}} \mathcal{E}_{\boldsymbol{x},\boldsymbol{\nu}} \left[\operatorname{trace}\left\{ \boldsymbol{W} \mathbf{F}^{-1}(\boldsymbol{x}, \boldsymbol{\nu}, \boldsymbol{P}) \right\} \right]$$

- $\boldsymbol{W}$ is a diagonal weighting matrix that emphasizes parameter(s) of interest (e.g., myelin water exchange $\tau_{\mathrm{f}\to\mathrm{s}}$).
- $\mathcal{E}_{\boldsymbol{x},\boldsymbol{\nu}}$ denotes expectation w.r.t $\boldsymbol{x}$ and $\boldsymbol{\nu}$ over a tissue distribution (e.g., white matter).
- $\hat{\boldsymbol{P}}$ contains optimized acquisition parameters for the D bSSFP acquisitions.

Estimation using PERK[14]

- Fast and dictionary-free kernel-based nonlinear estimator ("shallow" machine learning)
- At testing time, collect acquired data and known parameters per-voxel $\boldsymbol{q} := [|\boldsymbol{y}|^T, \, \boldsymbol{\nu}^T]^T \in \mathbb{R}^{D+K}$ (e.g., D = 40, K = 2).
- PERK estimates:

$$\hat{\mathbf{x}}(\boldsymbol{q}) = \boldsymbol{X}\left(\frac{1}{N}\mathbf{1}_N + \boldsymbol{M}(\boldsymbol{MKM} + \rho N \boldsymbol{I}_N)^{-1}\boldsymbol{k}(\boldsymbol{q})\right)$$

Notation: $\boldsymbol{X}$- training data, $\boldsymbol{K}$- kernel matrix, $\boldsymbol{k}(\cdot)$ - kernel function, $\boldsymbol{M}$- de-meaning operator, N - number of training points, ρ - PERK parameter, $|\boldsymbol{y}|$ - acquired magnitude data, $\boldsymbol{\nu}$ - known parameters

[14] G. Nataraj et al., *IEEE TMI*, 2018.

Setup:

- Opt. variables: α and ϕ values of 40 bSSFP scans; opt. time of $\sim$ 20hrs
- Flip angles α allowed to vary between 10° and 40°
- $T_\mathrm{R}/T_\mathrm{E}$ kept fixed to 20ms / 4ms
- Noise std. dev. of 3.867e-4 ($\sim$ 50dB image SNR)
- Scan design performed for tissue distributions centered around white matter; PERK is trained using a wider range.

Experiments

Setup:

- Opt. variables: α and ϕ values of 40 bSSFP scans; opt. time of $\sim$ 20hrs
- Flip angles α allowed to vary between 10° and 40°
- $T_{\mathrm{R}}/T_{\mathrm{E}}$ kept fixed to 20ms / 4ms
- Noise std. dev. of 3.867e-4 ($\sim$ 50dB image SNR)
- Scan design performed for tissue distributions centered around white matter; PERK is trained using a wider range.

Metric:

$$\text{Coefficient of variation} = \frac{\sqrt{\text{Cramér-Rao bound}}}{\text{mean value of parameter}}$$

Tissue distributions

Parameter	Distributions for scan design	PERK training ranges
M_0	$\mathrm{Unif}(0.769, 0.771)$	$\mathrm{Unif}(0.75, 1.0)$
f_{f}	$\mathrm{Unif}(0.149, 0.151)$	$\mathrm{Unif}(0.03, 0.31)$
$T_{1\mathrm{f}}$ (in ms)	$\mathrm{Unif}(399, 401)$	$\mathrm{Unif}(300, 500)$
$T_{1\mathrm{s}}$ (in ms)	$\mathrm{Unif}(831, 833)$	$\mathrm{Unif}(800, 1350)$
$T_{2\mathrm{f}}$ (in ms)	$\mathrm{Unif}(19.9, 20.1)$	$\mathrm{Unif}(16, 24)$
$T_{2\mathrm{s}}$ (in ms)	$\mathrm{Unif}(79.9, 80.1)$	$\mathrm{Unif}(64, 96)$
$\tau_{\mathrm{f}\to\mathrm{s}}$ (in ms)	$\mathrm{Unif}(50, 250)$	$\mathrm{Unif}(50, 250)$
$\Delta\omega_{\mathrm{f}}$ (in Hz)	$\mathrm{Unif}(0, 10)$	$\mathrm{Unif}(0, 10)$
$\Delta\omega$ (in Hz)	$\mathrm{Unif}(-25, 25)$	$\mathrm{Unif}(-25, 25)$
κ	$\mathrm{Unif}(0.8, 1.2)$	$\mathrm{Unif}(0.8, 1.2)$

- Narrow tissue distributions centered around white matter[15] for scan design

[15] S. T. Whitaker et al., *MRM*, 2020. [17]

Optimized bSSFP scans: signal profiles

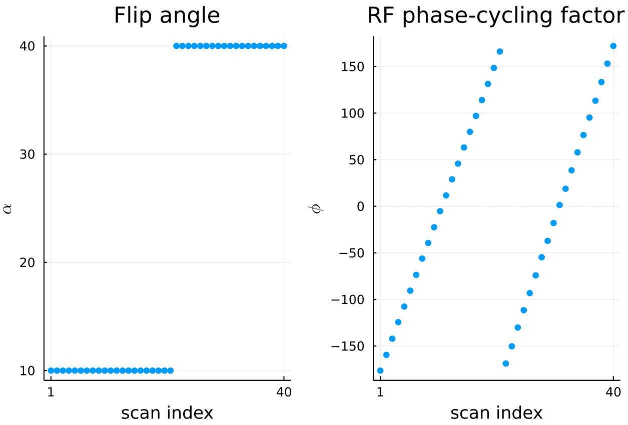

- Curiously regular set of optimized ϕ factors across the 40 bSSFP scans

Note: We *reordered* the 40 acquisitions for visualization purposes.

Optimized bSSFP scans: signal profiles

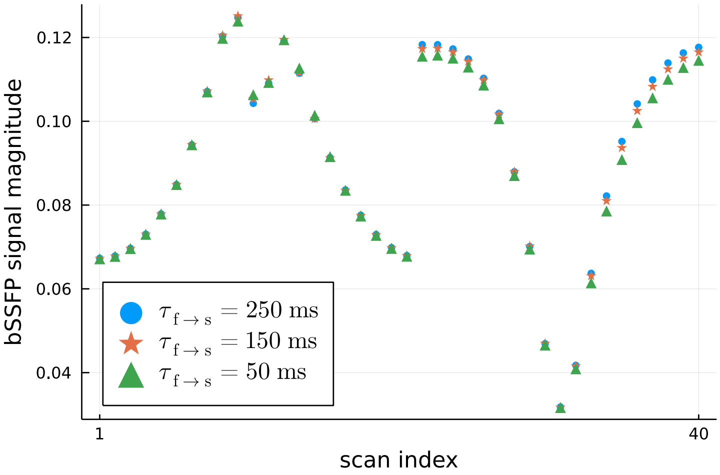

- Predicted coeff. of var. of $\sim$ **13%** for estimating exchange in white matter (WM).

Varying off-resonance

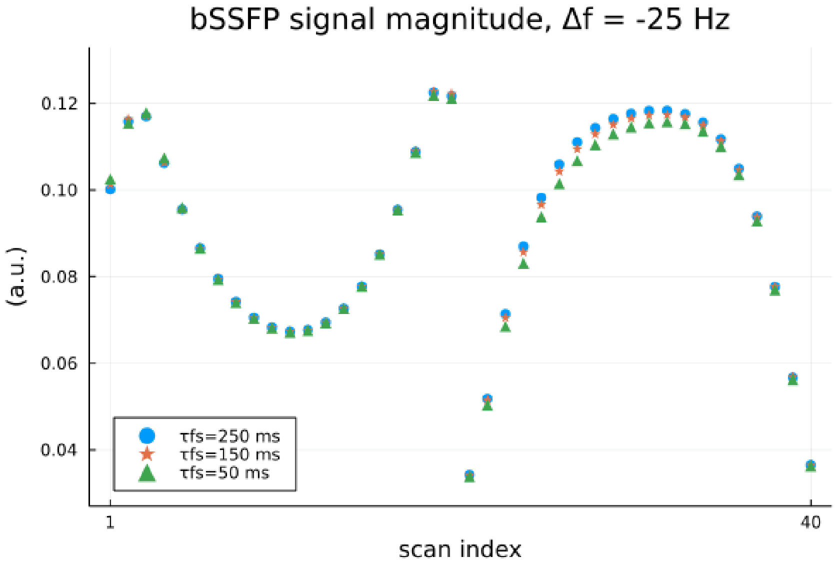

Importance of optimizing ϕ factors

Experiment	Coeff. of variation
optimizing T_R, α and ϕ	0.13
optimizing α and ϕ	**0.13**
optimizing T_R and α	0.58
optimizing only α	561.8

- Optimizing the RF phase cycling factors ϕ yielded the biggest reduction in coefficient of variation for estimating exchange in WM.

Numerical simulations (BrainWeb[17])

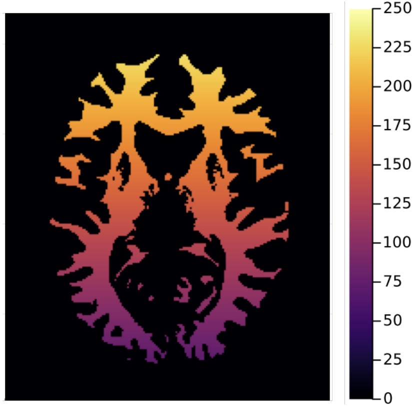

Ground truth exchange map $\tau_{\mathrm{f}\to\mathrm{s}}$ [ms]

- Digital phantom used to simulate optimized set of 40 bSSFP scans
- Assigned tissue parameters for WM (from literature[16])
- Exchange varies anterior-to-posterior; off-resonance from left-to-right

[16] S. T. Whitaker et al., *MRM*, 2020.
[17] D. L. Collins et al., *IEEE TMI*, 1998. [18]

Numerical simulations - Results

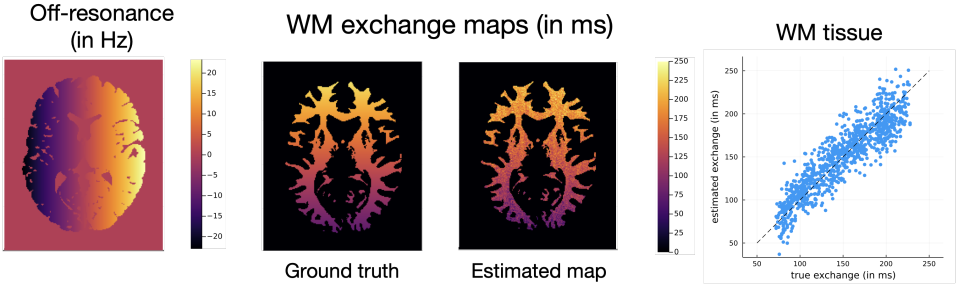

- Estimated exchange map has an RMSE of $\sim$ **12.5%** in WM.
- Exchange estimates are unreliable in grey matter (GM); it has very low myelin content.

In vivo acquisitions

- 40 bSSFP scans;
  separate Bloch-Siegert and SPGR scans to estimate B_0 and B_1+ maps
- FOV: $240 \times 200 \times 24$ mm^3; Matrix size: $192 \times 168 \times 8$
- Total scan time: $\sim$ 10 minutes (fully sampled)
- 32-channel data; magnitude data obtained using root-sum-of-squares method

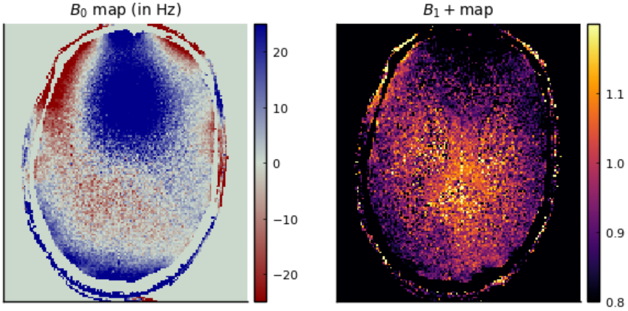

bSSFP magnitude images (slice 3)

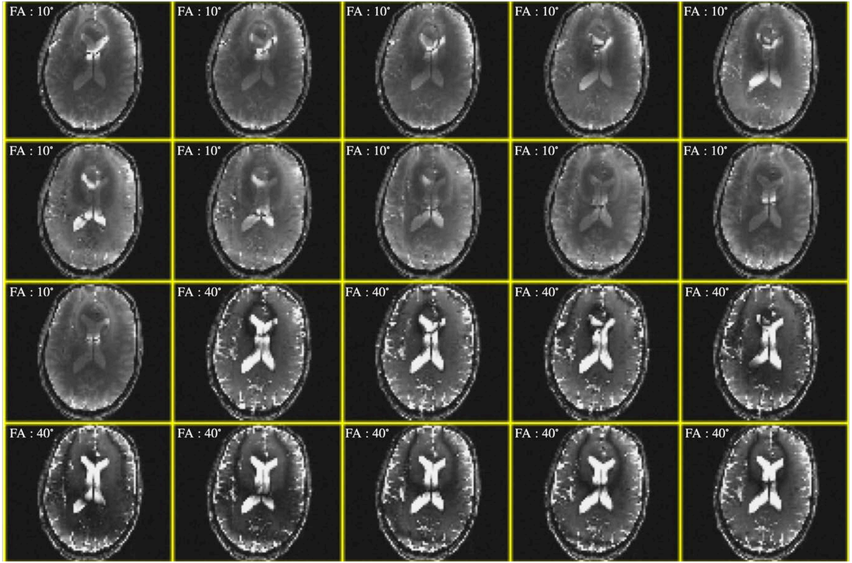

Estimated exchange map $\tau_{\mathrm{f}\to\mathrm{s}}$

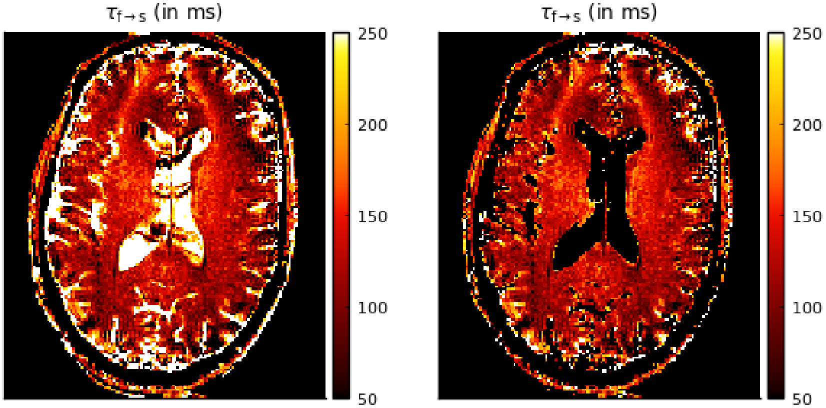

Exchange map without (*left*) and with (*right*) CSF masking

Other parameter estimates

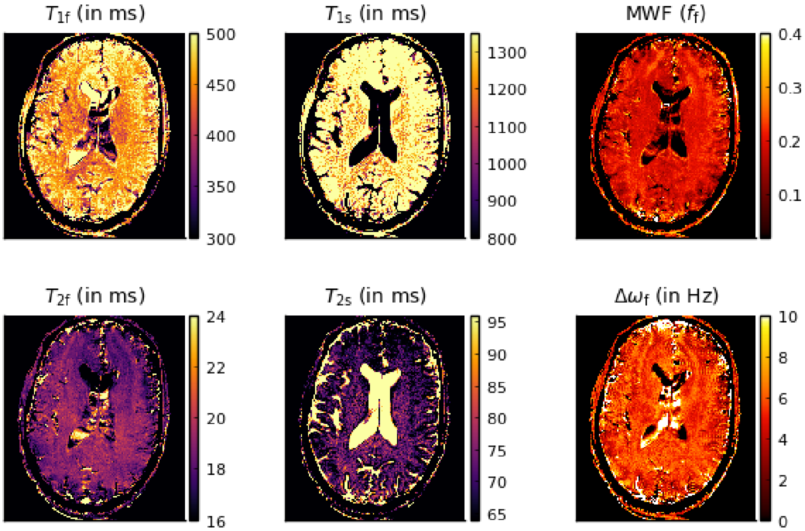

Sensitivity to off-resonance $\Delta\omega$

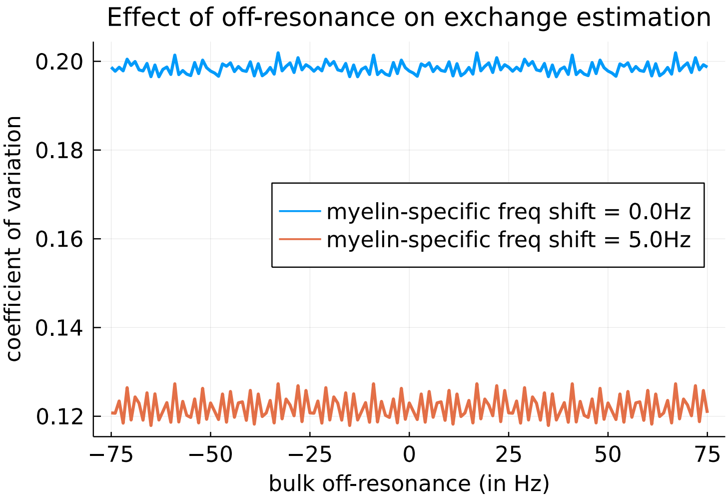

- Predicted coefficient of variation for estimating exchange in WM remains uniform with off-resonance.

Sensitivity to myelin-specific frequency shift $\Delta\omega_f$

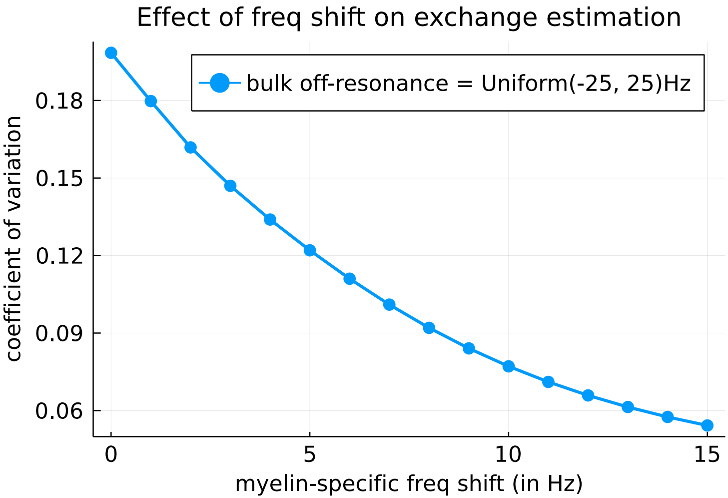

- Predicted coefficient of variation for estimating exchange in WM improves as $\Delta\omega_f$ increases.

Effects of main field B_0 drift (WIP)

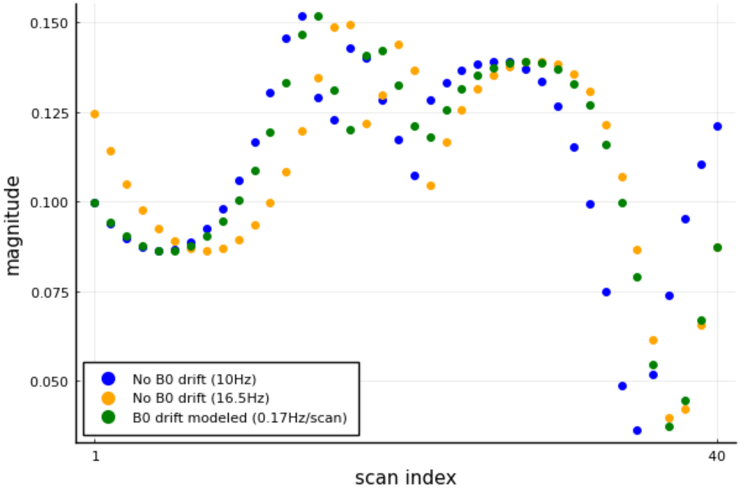

≈ 1 Hz/min drift $\Longrightarrow \approx 6.5$ Hz drift over 40 scans[18]

[18] T. Benner, *MRM*, 2006. [19]

Optimized bSSFP+PERK without drift

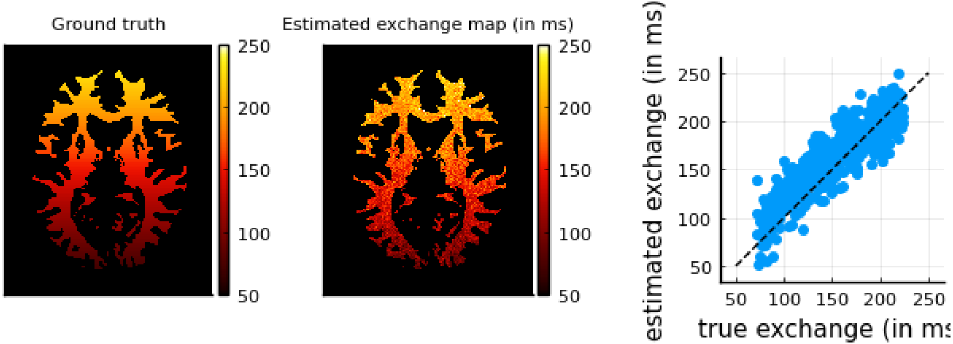

Optimized bSSFP+PERK, but with (unknown) drift

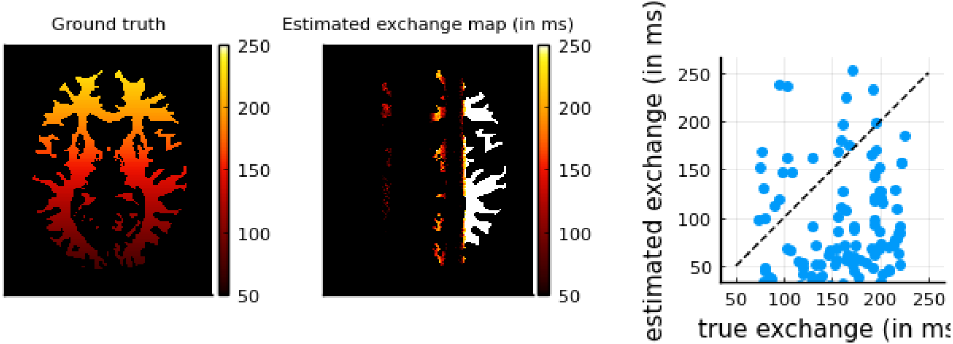

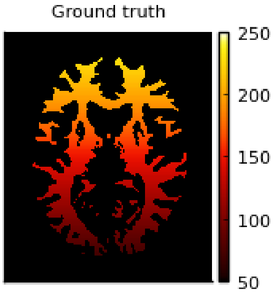
Ground truth
250
200
150
100
50

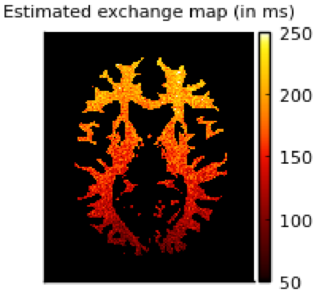
Estimated exchange map (in ms)
250
200
150
100
50

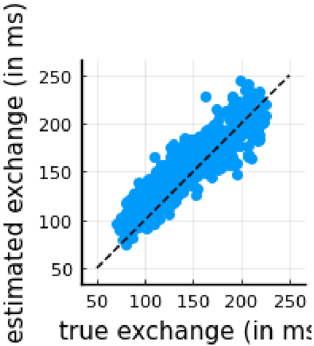
estimated exchange (in ms)
250
200
150
100
50
50
100
150
200
250
true exchange (in ms

Summary

- Optimized bSSFP scans have the potential to quantify exchange in white matter.
- Using a range of phase-cycling increment factors seems crucial.
- Modeling drift (or accelerating scans) seems important.

Validation of exchange maps

- Validate the optimized bSSFP design in a urea-based phantom using Relaxation Exchange Spectroscopy (REXSY)[19].
- Examine through-voxel B_0 gradient effects (T_2^*)

Transient data

- Acquire data during the transient period of each bSSFP acquisition; transient + steady-state data could improve exchange estimates.

Maximum-likelihood estimator

- Compare PERK-based parameter estimates with ML estimates.

[19] R. D. Dortch et al., *J. Chem. Phys.*, 2009. [20]

Resources

Talk and code available online at
`http://web.eecs.umich.edu/~fessler`

Bibliography I

[1] G. Wang, T. Luo, J-F. Nielsen, D. C. Noll, and J. A. Fessler. "B-spline parameterized joint optimization of reconstruction and k-space trajectories (BJORK) for accelerated 2D MRI." In: *IEEE Trans. Med. Imag.* 41.9 (Sept. 2022), 2318–30.

[2] G. Wang, T. Luo, J-F. Nielsen, D. C. Noll, and J. A. Fessler. *B-spline parameterized joint optimization of reconstruction and k-space trajectories (BJORK) for accelerated 2D MRI*. 2021.

[3] N. Murthy, J-F. Nielsen, S. T. Whitaker, M. W. Haskell, S. D. Swanson, N. Seiberlich, and J. A. Fessler. "Quantifying exchange using optimized bSSFP sequences." In: *Proc. Intl. Soc. Mag. Res. Med.* 2022, p. 2068.

[4] Y. Jiang, D. Ma, N. Seiberlich, V. Gulani, and M. A. Griswold. "MR fingerprinting using fast imaging with steady state precession (FISP) with spiral readout." In: *Mag. Res. Med.* 74.6 (Dec. 2015), 1621–31.

[5] D. C. Dean, J. Sojkova, S. Hurley, S. Kecskemeti, O. Okonkwo, B. B. Bendlin, F. Theisen, S. C. Johnson, A. L. Alexander, and C. L. Gallagher. "Alterations of myelin content in Parkinson's disease: A cross-sectional neuroimaging study." In: *PLoS One* 11.10 (2016), 1–20.

[6] G. F. Piredda, T. Hilbert, J-P. Thiran, and T. Kober. "Probing myelin content of the human brain with MRI: A review." In: *Mag. Res. Med.* 85.2 (Feb. 2021), 627–52.

[7] W. Huang, . X. Li, . E. A. Morris, . L. A. Tudorica, . V. E. Seshan, . W. D. Rooney, . I. Tagge, . Y. Wang, . J. Xu, and . C. S. Springer. "The magnetic resonance shutter speed discriminates vascular properties of malignant and benign breast tumors in vivo." In: *Proc. Natl. Acad. Sci.* 105.46 (Nov. 2008), 17943–8.

[8] S. Kim, H. Quon, L. A. Loevner, M. A. Rosen, L. Dougherty, A. M. Kilger, J. D. Glickson, and H. Poptani. "Transcytolemmal water exchange in pharmacokinetic analysis of dynamic contrast-enhanced MRI data in squamous cell carcinoma of the head and neck." In: *J. Mag. Res. Im.* 26.6 (Dec. 2007), 1607–17.

[9] A. N. Dula, D. F. Gochberg, H. L. Valentine, W. M. Valentine, and M. D. Does. "Multiexponential T2, magnetization transfer, and quantitative histology in white matter tracts of rat spinal cord." In: *Mag. Res. Med.* 63.4 (Apr. 2010), 902–9.

[10] K. D. Harkins, A. N. Dula, and M. D. Does. "Effect of intercompartmental water exchange on the apparent myelin water fraction in multiexponential T2 measurements of rat spinal cord." In: *Mag. Res. Med.* 67.3 (2012), 793–800.

[11] S. C. L. Deoni, B. K. Rutt, T. Arun, C. Pierpaoli, and D. K. Jones. "Gleaning multicomponent T1 and T2 information from steady-state imaging data." In: *Mag. Res. Med.* 60.6 (Dec. 2008), 1372–87.

[12] J. I. Hamilton, A. Deshmane, M. Griswold, and N. Seiberlich. "MR fingerprinting with chemical exchange (MRF-X) for in vivo multi-compartment relaxation and exchange rate mapping." In: *Proc. Intl. Soc. Mag. Res. Med.* 2016, p. 0431.

[13] R. D. Dortch, K. D. Harkins, M. R. Juttukonda, J. C. Gore, and M. D. Does. "Characterizing inter-compartmental water exchange in myelinated tissue using relaxation exchange spectroscopy." In: *Mag. Res. Med.* 70.5 (Nov. 2013), 1450–9.

[14] C. Laule and G. R. W. Moore. "Myelin water imaging to detect demyelination and remyelination and its validation in pathology." In: *Brain Pathology* 28.5 (Sept. 2018), 750–64.

[15] S. Wharton and R. Bowtell. "Fiber orientation-dependent white matter contrast in gradient echo MRI." In: *Proc. Natl. Acad. Sci.* 109.45 (Nov. 2012), 18559–64.

[16] G. Nataraj, J-F. Nielsen, C. D. Scott, and J. A. Fessler. "Dictionary-free MRI PERK: Parameter estimation via regression with kernels." In: *IEEE Trans. Med. Imag.* 37.9 (Sept. 2018), 2103–14.

[17] S. T. Whitaker, G. Nataraj, J-F. Nielsen, and J. A. Fessler. "Myelin water fraction estimation using small-tip fast recovery MRI." In: *Mag. Res. Med.* 84.4 (Oct. 2020), 1977–90.

[18] D. L. Collins, A. P. Zijdenbos, V. Kollokian, J. G. Sled, N. J. Kabani, C. J. Holmes, and A. C. Evans. "Design and construction of a realistic digital brain phantom." In: *IEEE Trans. Med. Imag.* 17.3 (June 1998), 463–8.

[19] T. Benner, Andre J W van der Kouwe, J. E. Kirsch, and A. G. Sorensen. "Real-time RF pulse adjustment for B0 drift correction." In: *Mag. Res. Med.* 56.1 (July 2006), 204–9.

[20] R. D. Dortch, R. A, Horch, M. D, and Does. "Development, simulation, and validation of NMR relaxation-based exchange measurements." In: *J. Chem. Phys.* 131.16 (Oct. 2009), p. 164502.

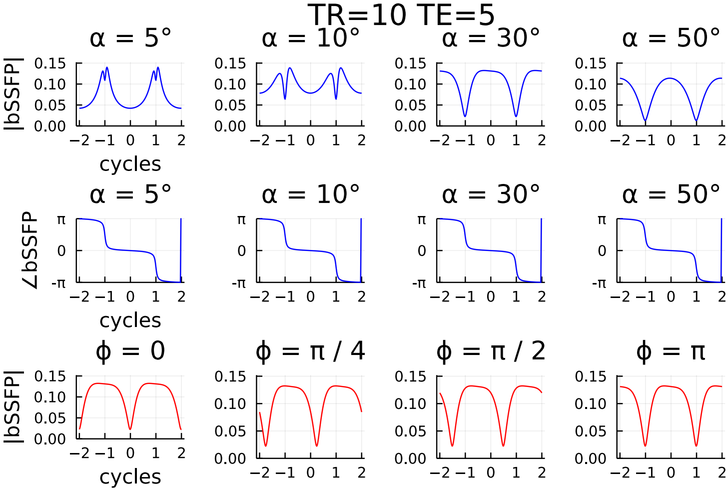
TR=10 TE=5
α = 5°
α = 10°
α = 30°
α = 50°
|bSSFP|
0.15
0.10
0.05
0.00
−2 −1 0 1 2
cycles
∠bSSFP
π
0
-π
ϕ = 0
ϕ = π / 4
ϕ = π / 2
ϕ = π

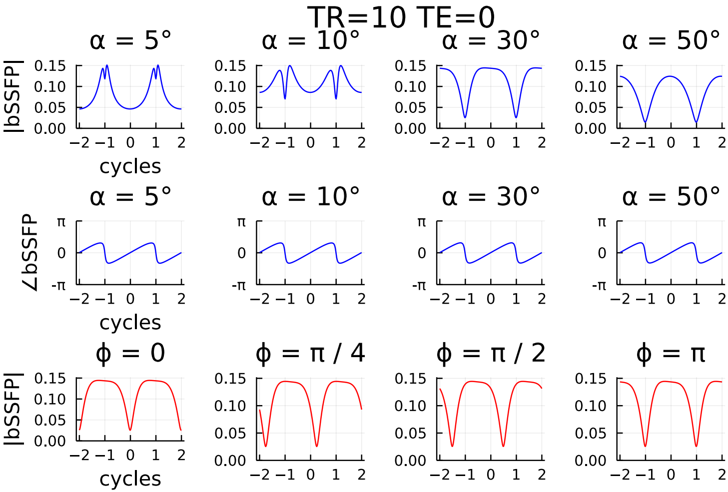
TR=10 TE=0
α = 5°
α = 10°
α = 30°
α = 50°
|bSSFP|
0.15
0.10
0.05
0.00
−2 −1 0 1 2
cycles
∠bSSFP
π
0
-π
ϕ = 0
ϕ = π / 4
ϕ = π / 2
ϕ = π